Controlling the formation of a monolayer of cytochrome P450 reductase onto Au surfaces

J. H. Convery,[1] C. I. Smith,[1] B. Khara,[2] N. S. Scrutton,[2] P. Harrison,[1] T. Farrell,[1] D. S. Martin,[1] and P. Weightman[1,*]

[1]*Department of Physics, Oliver Lodge Laboratory, University of Liverpool, Liverpool L69 7ZE, United Kingdom*

[2]*Faculty of Life Sciences, University of Manchester, Manchester Interdisciplinary Biocentre, 131 Princess Street, Manchester M1 7ND, United Kingdom*

(Received 24 November 2011; published 3 July 2012)

The conditions necessary for the formation of a monolayer and a bilayer of a mutated form (P499C) of human cytochrome P450 reductase on a Au(110)/electrolyte interface have been determined using a quartz crystal microbalance with dissipation, atomic force microscopy, and reflection anisotropy spectroscopy (RAS). The molecules adsorb through a Au-S linkage and, for the monolayer, adopt an ordered structure on the Au(110) substrate in which the optical axes of the dipoles contributing to the RAS signal are aligned roughly along the optical axes of the Au(110) substrate. Differences between the absorption spectrum of the molecules in a solution and the RAS profile of the adsorbed monolayer are attributed to surface order in the orientation of dipoles that contribute in the low energy region of the spectrum, a roughly vertical orientation on the surface of the long axes of the isoalloxazine rings and the lack of any preferred orientation in the molecular structure of the dipoles in the aromatic amino acids. Our studies establish an important proof of principle for immobilizing large biological macromolecules to gold surfaces. This opens up detailed studies of the dynamics of biological macromolecules by RAS, which have general applications in studies of biological redox chemistry that are coupled to protein dynamics.

DOI: 10.1103/PhysRevE.86.011903 PACS number(s): 87.14.E−

I. INTRODUCTION

Nicotinamide adenine dinucleotide phosphate hydrogen (NADPH)-dependent cytochrome P450 reductase (CPR) is an important mammalian enzyme required to deliver electrons to cytochrome P450 enzymes, which catalyze the detoxification of a wide range of xenobiotics and drugs [1]. The enzyme (Fig. 1) is modular in construction, comprising distinct redox domains each bound to a flavin cofactor, which are successfully oxidized and reduced as part of the natural catalytic cycle [2]. The crystallographic structure of CPR suggests that the enzyme is dynamic and that domain motion might accompany electron transfer and the interaction of CPR with P450 partner proteins [3]. These dynamic models for catalysis have been corroborated through small angle x-ray scattering studies, pulsed electron-electron double resonance spectroscopy, and high pressure and temperature jump studies of the kinetics of interflavin electron transfer [4–6]. Fluorescence energy transfer studies of an engineered form of CPR performed during substrate oxidation have also emphasized the strong coupling of protein motion to changes in redox chemistry [7]. Despite strong evidence to suggest that protein motion is coupled to electron transfer in CPR, direct observation of motion is challenging, and previous studies have concentrated on the dynamic properties of CPR in a dilute solution. In the cell, CPR is tethered to the membrane of the microsomal endoplasmic reticulum where the degree of macromolecular crowding is significant. Here, cellular protein concentrations are typically 10^3–10^4 greater than used routinely in laboratory-based biophysical measurements. The tethering and crowding of CPR at the endoplasmic reticulum will likely change the dynamic properties of the protein with consequent impact on microsomal electron transfer chemistry [7]. In principle, reflection anistropy spectroscopy (RAS) measurements would allow the study of the redox chemistry and dynamic properties of CPR as a monolayer of protein adsorbed at Au(110)/electrolyte interfaces, mimicking more closely conditions found in the cell. The development of RAS-based methods to investigate CPR motion (and, by analogy, other protein systems) within the confines of a crowded tethered monolayer is the motivation for our paper.

In an earlier paper [8], we demonstrated that monitoring the RAS of electron transfer flavoproteins (ETFs) adsorbed at Au(110)/electrolyte interfaces provided insight into the conformational changes that accompany the transfer of electrons. The success of this approach established that the ETFs formed ordered structures at the Au(110)/electrolyte interface and that this could be used to investigate the dynamic behavior of such systems. In this paper, we establish the conditions under which ordered monolayers and bilayers of cytochrome P450 reductase (Fig. 1) form at Au(110)/electrolyte interfaces. We find that the optical axes of the molecules in an adsorbed monolayer are aligned along the optical axes of the Au(110) surface. Establishing the conditions under which a monolayer of cytochrome P450 reductase forms on the Au(110)/electrolyte interface is an important first step in the study of the dynamic behavior of this protein using RAS. The development of methods to study protein dynamics coupled to biological redox chemistry is very challenging, and to date, there are no readily accessible real-time methods for studying motions linked to redox chemistry and biological function that can be applied to proteins in general (whether soluble or membrane associated). We show here that RAS opens up this possibility. Consequently, it is crucial that methods are established to functionalize Au surfaces that enable real-time measurement of protein motion during reversible reduction

*Author to whom correspondence may be addressed: peterw@liverpool.ac.uk

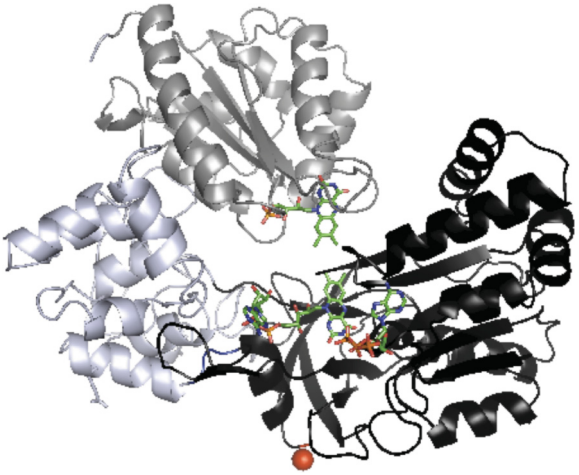

FIG. 1. (Color online) Molecular graphics ribbon diagram representation for the structure of cytochrome P450 reductase. The sphere indicates the location of the Pro-499 residue that was targeted by site-directed mutagenesis to produce the P499C variant. The flavin mononucleotide- (FMN)-binding domain is shown in dark gray, the connecting domain in light gray, and the flavin adenine dinucleotide (FAD)/NADP domain in black. The FAD and FMN cofactors are shown as sticks.

and oxidation of the protein cofactors using electrochemistry. We have accomplished this with CPR, a structurally and functionally well-characterized human protein where large-scale domain motion is known to be associated with electron transfer. Moreover, this is a membrane-associated protein, and thus, we have also established the principle of working with "difficult" membrane-associated proteins as well as soluble proteins on the Au surface. Our paper provides a proof-of-principle concept that will enable the use of RAS to study dynamics coupled to biological redox reactions. The study will also enable analysis of behavior on more functionalized Au surfaces (e.g., protein coadsorbed with membrane fatty acids) to mimic natural biological membranes.

II. EXPERIMENTAL SECTION

The variant form (Pro-499 to Cys-499, P499C) of human CPR was obtained by site-directed mutagenesis using the following "forward" and "reverse" oligonucleotide primers: 5′-CTG CGG GCC AAG GAG TGC GCC GGG GAG AAC GGC-3′, P499C reverse, 5′-GCC GTT CTC CCC GGC GCA CTC CTT GGC CCG CAG-3′, and the Quikchange site-directed mutagenesis kit (Stratagene, UK). The mutated gene was completely sequenced to verify that no spurious changes had arisen during the mutagenesis procedure. Human CPR was overexpressed in BL21 (DE3) pLysS and was purified using Ni^{2+}-NTA agarose, followed by Q-Sepharose ion-exchange chromatography according to published procedures [2]. During purification of CPR, the buffer (100 mM potassium phosphate, *p*H 7.2) was supplemented with 2-mercaptoethanol (2 mM) to maintain the reduced form of the engineered cysteine residues. For longer term storage, 2-mercaptoethanol was replaced by dithiothreitol [(DTT), 2 mM]. Prior to immobilization on the Au surface, 2-mercaptoethanol and DTT were removed from the protein solution by rapid gel filtration. Enzyme concentration was determined spectroscopically using extinction coefficients of 22 $mM^{-1}\,cm^{-1}$ at 454 nm for full-length CPR [2] and 11 $mM^{-1}\,cm^{-1}$ at 450 nm for the individual FAD/NADPH- and FMN-binding domains. The positioning of the engineered cysteine residues on the solvent accessible surface of human CPR was guided by reference to the x-ray crystallographic structure of the homologous rat enzyme [3]. The dithiothreitol was removed by eluting on a column immediately prior to use in the experiments. Some experiments were also performed on the wild-type form of human cytochrome P450 reductase, which was prepared as described for the P499C variant but in the absence of exogenous thiol reductant.

The experiments employed a range of experimental techniques: quartz crystal microbalance with dissipation (QCM-D), atomic force microscopy (AFM), a standard RAS instrument of the Aspnes design [9], and a rapid RAS instrument [10] to understand the adsorption process for the protein.

The concentration and *p*H of the solution were found to be major determinants of the formation of adsorbed monolayers and bilayers at the Au/electrolyte interfaces. These conditions were established with a Q-Sense E4 module (Biolin Scientific) QCM-D. Polished polycrystalline Au substrates AT-cut 5 MHz crystals were treated in a UV ozone chamber for 10 min before being mounted inside the flow module and then placed into the E4 temperature controlled unit at 20 °C. Q-SOFT 401 software was used to acquire the frequency (f) and dissipation (D) data, which were analyzed using Q-TOOLS 3.0 (Biolin Scientific). Ultrapure water was initially pumped over the sensors for at least 30 min until a steady trace for frequency and dissipation were obtained. This procedure was then repeated for a phosphate buffer solution (0.1M NaH_2PO_4-K_2HPO_4). The baseline was recorded for 2 min, and then protein samples were flowed over the sensors for 5 min at 100 μl/min. The pump rate was then reduced to 10 μl/min for a further 25 min, and finally, the excess protein solution was removed by rinsing with a buffer for an hour. The observed changes in frequency can be related to the amount of mass adsorbed on the electrode using the Sauerbrey relationship [11] for rigid evenly distributed thin layers. However, for soft viscoelastic films, such as those studied here, a more accurate film thickness can be estimated by simultaneously measuring the change in frequency and dissipation of the sensor. The Voigt model [12] is then used, which relates thickness, density, sheer, and viscosity to give a much more accurate and realistic measure of the layer thickness.

Cytochrome P450 reductase was also adsorbed onto a Au(110) single crystal in an electrochemical cell. The Au(110) single crystal of 99.999% purity in the form of a disk of diameter 10 mm and 2 mm thick with an exposed surface area of 0.5 cm^2 was employed. The crystal was orientated to an accuracy of 0.1° by x-ray diffraction. The crystal was then prepared for each experiment by mechanically polishing on successively smaller grades of diamond paste down to 0.25 μm followed by flame annealing with a butane microtorch and protected with a drop of ultrapure water before being transferred into the electrochemical cell. The electrochemical cell used was a homemade three-electrode cell with a platinum counterelectrode, and a saturated calomel electrode (SCE) was used as the reference electrode. All potentials quoted

are referenced to the SCE. A silica strain free disk was used as the optical window in the cell. The potentiostat was an Autolab PGSTAT 30 with GPES software (Eco Chemie). The solutions used were NaH_2PO_4 and K_2HPO_4 (BDH, AnalaR grade) prepared with millipore ultrapure water (18 MΩ cm) and made oxygen free by purging with argon prior to use.

RAS is a linear optical technique in which the difference in reflectivity from two orthogonal directions in the surface of plane polarized light at normal incidence and reflection is measured. For a cubic substrate, this geometry results in a cancellation of the bulk signal by symmetry, and RAS becomes a probe of surface anisotropy. The technique was developed initially to probe the surfaces and growth of semiconductors [9,13–15] and has been recently reviewed [15]. In recent years, it has been applied to investigate the metal-liquid interface [16] and the adsorption of molecules onto surfaces in both UHV [17,18] and in liquid [19–22].

The RA spectrometer used in this and earlier [19–22] papers follows the Aspnes design [9]. The measured RA signal from 1.5 to 5.5 eV is given by

$$\mathrm{Re}\left(\frac{\Delta r}{r}\right) = \mathrm{Re}\ 2\left(\frac{r_{[1\bar{1}0]} - r_{[001]}}{r}\right), \qquad (1)$$

where $r_{[1\bar{1}0]}$ and $r_{[001]}$ are the reflection coefficents in the $[1\bar{1}0]$ and [001] directions, respectively, in the (110) surface and $r/2$ is the average of these quantities.

RAS is sensitive to the steps, surface states, and reconstructions of the Au(110) surface with the result that it is difficult to obtain reproducible results from the flame annealing process [16,23–25]. However, by careful attention to the duration and sequence of the flame annealing process, it is possible to achieve good reproducibility as may be seen from a comparison of the RAS observed from Au(110) surfaces used in earlier studies [19–22] and from the assignment of the RA spectra from each of the reconstructions on the Au(110) surface [26]. In this paper, almost identical RA spectra of the Au(110) crystal were obtained in two experiments in which the crystal was used as the substrate held at a potential of − 0.652 V for the deposition of a monolayer and a bilayer of cytochrome P450 reductase [Fig. 2(a)].

RAS results were also obtained with a 32 channel RA spectrometer developed from the 16 channel rapid RAS instrument described in detail earlier [10]. This instrument uses a 32 channel UV enhanced photodiode array (device number S4114-35Q, Hamamatsu) and collects spectra in parallel. Each channel is individually amplified and is digitized. The digitized signals are processed using phase locked, signal averaging, and fast Fourier transform techniques replacing the function of the lock-in amplifier on a standard RA instrument and without the need for 32 lock-in amplifiers [10]. The instrument was calibrated before each experiment using narrow bandpass filters of known wavelength to accurately establish the wavelength of each channel. The rapid RAS instrument operated over the range of 2.0–4.0 eV and yielded spectra for the Au(110) surface and the monolayer of cytochrome P450 reductase adsorbed on the Au(110) equivalent to those obtained with the standard instrument.

AFM was performed using a Nanoscope IIIa MultiMode instrument (Digital Instruments) in contact mode. Silicon nitride probes of nominal spring constant 0.35 N/m were used. Samples of known thickness were prepared in the QCM-D and then were imaged under a phosphate buffer solution within a liquid cell at room temperature. The contact force was minimized in order to minimize the applied force of the tip on the protein structures while maintaining proper tracking of the surface topography.

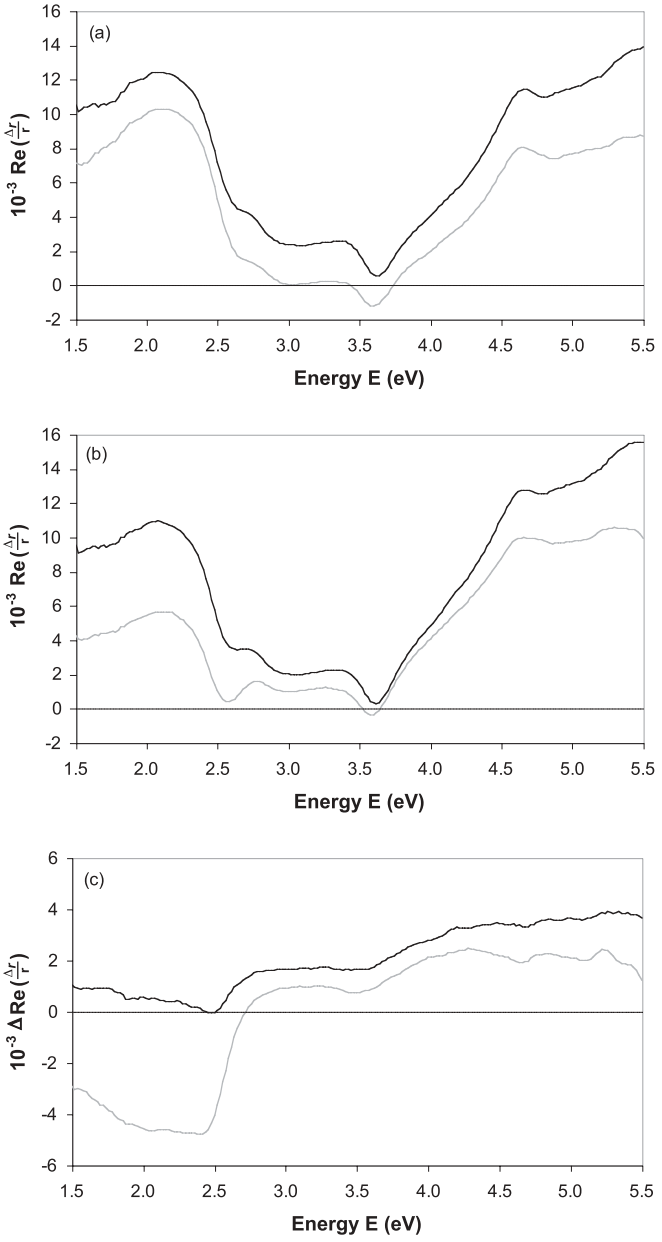

FIG. 2. RA spectra of (a) Au(110) at − 0.652 V, (b) Au(110) + P499C full-length CPR at − 0.652 V, and (c) P499C full-length CPR at − 0.652 V obtained by subtracting the corresponding Au(110) spectrum from the Au(110) + protein spectrum all recorded in 0.1*M* NaH_2PO_4-K_2HPO_4 (*p*H 7.2) black line: monolayer experiment and gray line: bilayer experiment. The RA spectra depicted by the black lines have all been shifted up by two units on the vertical axis, whereas, the gray lines correspond to the vertical scale. The spectra of the clean Au(110) surfaces differ slightly in the position of the origin in the vertical scale from previous work due to small differences in the position of the polarizer angle in the RAS instrument.

TABLE I. The redox potentials for the wild-type and the P499C variant of cytochrome P450 reductase are shown as well as possible sites of the electron, denoted by • in the P499C full-length CPR.

Redox potentials	Oxidized	1*e* reduced	2*e* reduced	3*e* reduced	4*e* reduced
Wild type	0.036 V	– 0.394 V	– 0.504 V	– 0.574 V	– 0.744 V
P499C	0.056 V	– 0.376 V	– 0.465 V	– 0.557 V	– 0.652 V
Possible redox states	FMN FAD	FMN FADH• FMNH• FAD	FMNH• FADH• FMN $FADH_2$ $FMNH_2$ FAD	FMNH• $FADH_2$ $FMNH_2$ FADH•	$FMNH_2$ $FADH_2$

III. RESULTS

Redox potentiometry conducted on both wild-type and variant P499C full-length CPR were measured electrochemically by redox titration as previously described [27]. The redox potentials for the flavin couples were calculated by global analysis of data obtained from reductive titrations of protein samples titrated against dithionite under anaerobic conditions and established that the reduction potentials of the flavin couples in the variant P499C CPR were not substantially different from those of the wild-type CPR protein (Table I).

Figure 3 shows the results obtained for the adsorption of the P449C protein on the polycrystalline Au substrates in the QCM-D using a solution of *p*H 7.2 as a function of protein concentration. As the concentration of protein is increased, the film thickness increases. The inset of Fig. 3 shows the frequency and dissipation changes as a function of time for two concentrations that give rise to a monolayer and bilayer, respectively. The bottom black curves are the result of the frequency changes, and the upper gray curves are the corresponding changes in dissipation both with respect to time. The frequency is related to the amount of mass adsorbed on the surface and gives a measure of the thickness of the adsorbed layer, whereas, the dissipation is a measure of the rigidity of the layer. The dimensions of the protein deduced from the crystal structure of rat CPR are 5.9, 5.2, and 5.1 nm [3] with 5.9 nm corresponding to the vertical dimension in Fig. 1. Combining these dimensions with the results of Fig. 3 indicates that, at low concentrations, a monolayer is adsorbed and that this forms a more rigid and compact structure than the

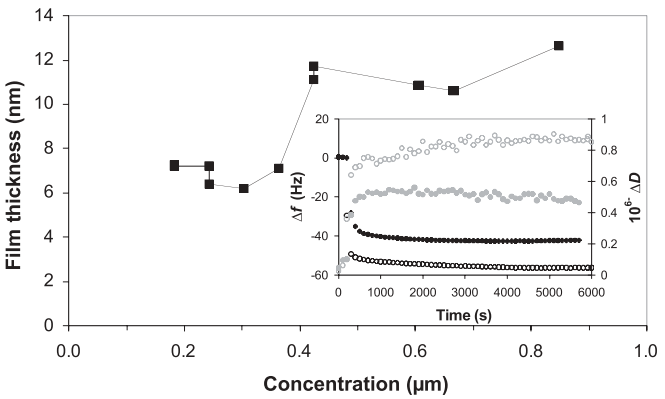

FIG. 3. Film thickness as a function of P499C full-length CPR concentration in 0.1 *M* NaH_2PO_4-K_2HPO_4 at *p*H 7.2. The inset shows the black: QCM-D frequency and gray: dissipation of (a) ●: 0.24 μM and (b) ◯: 0.85 μM, which correspond to film thicknesses of 7.2 and 12.6 nm, respectively.

bilayer which adsorbs at the higher concentrations. Identical conditions to those used for the QCM-D experiments were used to produce samples for AFM imaging, and the resulting images are shown in Fig. 4. The morphology of both films was of the type produced by molecular aggregates (Fig. 4). For the monolayer sample, the underlying Au substrate was exposed through small holes that were present occasionally in the monolayer and could be revealed by using the AFM tip to "scratch" away small areas of the protein layer. The aggregates were of height 4–6 nm measured from the Au substrate, which is consistent with the dimensions of the molecule as deduced from crystallography [3]. Although the AFM imaging was optimized to minimize the applied force on the substrate, the probe tip may compress the protein and may result in a reduced height being measured. Also, we note that the dimensions of a protein molecule, when adsorbed on a solid surface, may be different from the molecule dimensions as measured in crystallography.

An autocorrelation analysis [28] of the AFM images obtained for the monolayer sample showed weak striations directed along the diagonal of the square image [Fig. 4(b)]. A similar autocorrelation result was observed for the clean Au substrate, which displays a granular morphology of 1 to 2 nm height variation over areas of side length 2 μm. The autocorrelation result indicates that there is some self-similarity in both (i) the granular pattern of the clean substrate and (ii) the monolayer aggregates, along one particular direction over a length scale of a few micrometers. It appears that the substrate contributes to a localized ordering effect in the monolayer. No such pattern was observed for the bilayer, indicating that the effect is lost at this coverage. For the monolayer, the striation in the autocorrelation image is observed from areas of side length 1 to 2 μm [Fig. 4(b)], however, the effect is lost over larger areas. This area size gives an indication of the extent of the spatial correlation of the molecules on the polycrystalline Au surface.

For the bilayer, it was not possible to determine the location of the underlying Au substrate, however, aggregates having a maximum height of ∼8 nm were measured. The AFM results which show larger aggregate heights in the bilayer compared to those in the monolayer (Fig. 4) are in general agreement with the QCM-D results, which distinguish between monolayer and bilayer thicknesses.

The conditions under which monolayers and bilayers form depend quite sensitively on the *p*H and concentration of the solution as shown in Table II. These results show there is no simple relationship between the *p*H and the concentration at which a monolayer is formed but that, apart from the results at *p*H 7.0 and 7.8, the maximum concentration at

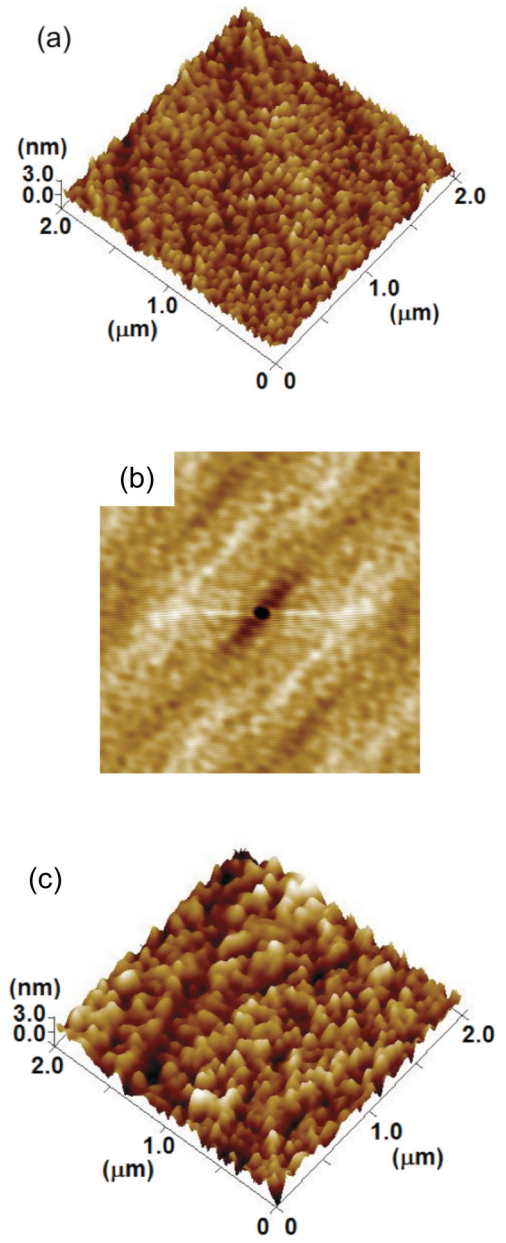

FIG. 4. (Color online) AFM images of a 2 μm $\times$ 2 μm area of a polycrystalline Au sensor obtained from the QCM-D after deposition of (a) monolayer, (b) the autocorrelation image obtained from the monolayer, and (c) bilayer film thickness.

which the adsorption is limited to a monolayer increases with increasing pH.

QCM-D studies of the adsorption of the wild type on the Au substrate at pH 7.2 always resulted in the formation of a bilayer or thicker films, and even reducing the concentration to 0.06 μM, the limit of detection in a solution with a UV-visible spectrometer failed to produce a monolayer.

Having established the conditions under which monolayers and bilayers of the mutant proteins adsorb on the polycrystalline Au substrates in the QCM-D, solutions of the appropriate pH and concentration were used in the electrochemical cell, and the adsorption was monitored on the Au(110) electrode with the potential held at -0.652 V, a potential which is known to result in the formation of

TABLE II. Summary of the QCM-D results showing the maximum concentration of P499C full-length CPR to achieve a monolayer as a function of solution pH.

pH	Concentration for monolayer adsorption (μM)
6.2	<0.36
6.8	<0.42
7.0	<0.24
7.2	<0.42
7.4	<0.67
7.8	<0.30

the Au(110)-(1 $\times$ 3) surface reconstruction [26]. Experience with small molecules, the S-containing amino acids [29], decanethiol [30], and a cysteine-tryptophan dimer [31], leads us to expect that the protein molecules (Fig. 1) will adsorb through the formation of a Au(110)-S linkage and that this will lead to a characteristic Au-S peak in the RAS at ~2.54 eV. We note that the protein contains several other cysteine residues, but none of these are on the outside of the molecule and so, unlike the engineered residue, are not available for bonding to the Au surface. The Au-S peak expected at 2.54 eV is observed in the RAS of both the monolayer and the bilayer systems as shown in Fig. 2(b) and is expected to overlap with the contribution from the molecules since, in a solution, the absorption spectrum of the proteins shows a rather broad feature in the range of 2.5–3.0 eV that is associated with the two isoalloxazine rings [32–36] (Fig. 5). While these results indicate that the engineered cysteine residues are involved in the bonding of the molecule to the surface, other residues may also be involved.

In order to characterize the adsorption process further, the rapid RAS instrument was used to monitor the spectral range of 2.0–4.0 eV in 32 channels simultaneously during adsorption. Selected adsorption curves obtained are shown in Fig. 6. From these data, it is clear that the adsorption curves at lower energies are significantly different from the adsorption curves obtained at higher energies. The adsorption curves obtained at 2.02, 2.25, and 2.53 eV show a strong decrease in the RAS signal, indicating adsorption between 500 and 1000 s

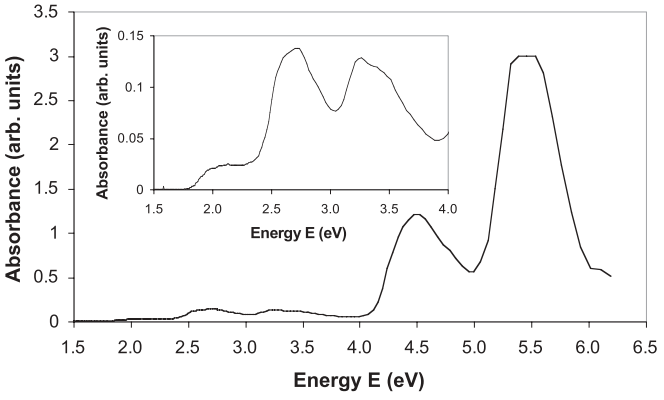

FIG. 5. UV-visible absorbance spectrum for 8.3 μM P499C full-length CPR in 0.1M NaH_2PO_4-K_2HPO_4 at pH 7.2 as a function of photon energy. The inset shows a blowup of the region 1.5–4.0 eV. Our results are in agreement with those of Ref. [34].

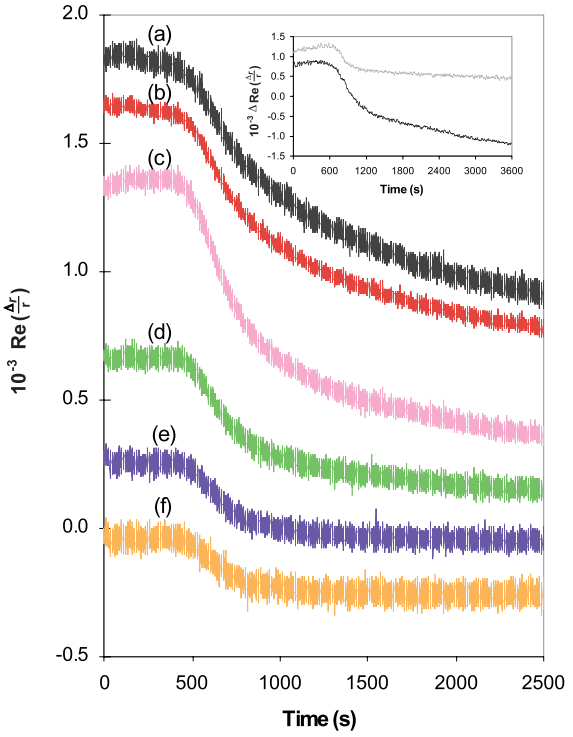

FIG. 6. (Color online) Changes in peak intensity as a function of time at (a) 2.02 eV, (b) 2.25 eV, (c) 2.53 eV, (d) 2.66 eV, (e) 2.73 eV, and (f) 3.06 eV measured in the rapid RAS instrument during the adsorption of P499C full-length CPR onto the Au(110) at -0.652 V in 0.1M NaH_2PO_4-K_2HPO_4 (pH 7.2). The inset shows the equivalent changes in the normal RAS instrument on two separately prepared Au(110) surfaces showing the intensity change at black line: 2.54 eV and gray line: 2.70 eV as a function of time. All the graphs correspond to the same intensity scale but are separated by arbitrary amounts on the vertical axis to prevent overlap.

followed by a much slower but steady decrease with time. However, the RAS signals obtained at higher energies show a similar initial decrease between 500 and 1000 s, but the signals then saturate. This behavior was replicated in separate adsorption experiments in which the RAS measured in the standard instrument was monitored as a function of time at 2.54 eV the energy of the Au-S bond and at 2.7 eV the peak of the absorption spectrum of the isoalloxazine rings. These results are shown in the inset of Fig. 6. This behavior provides a subtle insight into the adsorption process as will be discussed later.

A comparison of Figs. 2(a) and 2(b) shows that the RAS of the adsorbed molecules is strongly influenced by that of the RAS of the Au(110) substrate. The main differences from the RAS of Au(110) being an enhanced intensity in the low energy region and the presence of the peak at ~2.54 eV are associated with the formation of a Au-S bond. As in previous papers [19–22], we assume that the RAS of the adsorbed molecules is the sum of the contribution from the molecules and the RAS of the Au(110), and Fig. 2(c) shows the difference between these two contributions, which we attribute the RAS of the adsorbed species. This shows that the RASs of the monolayer and bilayer are very similar with the main difference between them being a much stronger contribution in the low energy

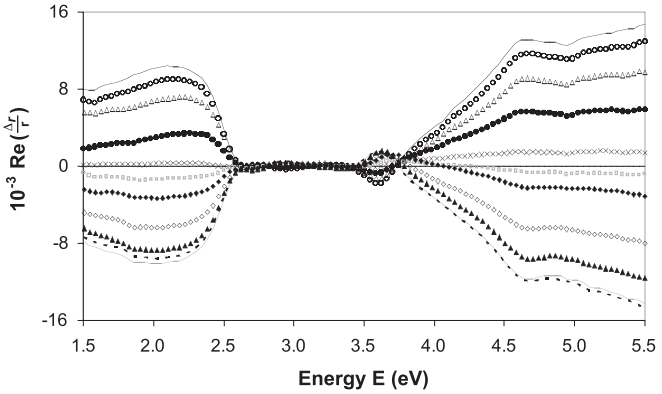

FIG. 7. RA spectra of Au(110) + P499C full-length CPR at -0.652 V in 0.1M $NaH_2PO_4 - K_2HPO_4$ (pH 7.2) as a function of azimuthal angle defined with respect to the Au [001] axis. Recorded at black line: 45°; ◯: 55°; △: 65°; ●: 75°; ×: 85°; □: 90°; ♦: 95°; ◇: 105°; ▲: 115°; gray line: 125°; and dashed line: 135°. When the spectrum obtained at 45° is plotted on the same vertical scale as Fig. 2(b), the two spectra are equivalent.

region and a much stronger peak at ~2.54 eV in the RAS of the bilayer.

In previous papers, we have shown that considerable insight into the orientation of adsorbed molecules on surfaces can be obtained by collecting RA spectra as a function of the azimuthal angle around the incident light beam [19–22]. Figure 7 shows the RAS obtained as a function of the azimuthal angle for the adsorbed monolayer. The spectra are essentially flat when measured along the principal axes of the Au(110) surface.

IV. DISCUSSION

The AFM results support the conclusions deduced from the QCM-D studies of the pH and concentration conditions required to form adsorbed monolayers and bilayers on polycrystalline Au. The autocorrelation analysis of the AFM results, obtained from the adsorbed monolayer, also show that the molecules tend to form ordered structures even on a polycrystalline surface. This suggests that there is a strong tendency of the interactions between adsorbed molecules to lead to ordered structures.

The failure of the wild type to produce an adsorbed monolayer suggests that the monolayers formed by the mutants arise from an interaction between the molecules and the surface mediated through the formation of a Au-S bond. This is supported by the observation of the characteristic Au-S feature in the RAS at ~2.54 eV (Fig. 2) and a consideration of the RAS measurements of the adsorption kinetics (Fig. 6). Even though the spectral feature associated with the Au-S bond overlaps with the spectrum of the isoalloxazine rings [32–36], there is a clear difference in adsorption kinetics at 2.54 and 2.7 eV as can be clearly seen in the inset of Fig. 6. RAS is a local probe that depends on macroscopic anisotropy. The intensity of a feature in the RA spectrum is a product of the intrinsic strength of the feature, the number of dipoles giving rise to the feature, and the degree of anisotropy. The kinetic behavior observed at 2.54 eV has been observed previously in the RAS of pyridine

adsorbed on Au(110) [37] and has been interpreted as an initial saturation of the surface followed by a much slower ordering process of the adsorbed species that increases the anisotropy. The adsorption kinetics observed at energies below 2.54 eV in Fig. 6 implies that the slower ordering that follows the initial adsorption of a monolayer increases the negative strength of the RAS signal due to an increase in anisotropy. However, this slow ordering does not change the strength of the RAS signal at higher energies. A possible explanation of this behavior is that the ordering process does not change the net orientation of the dipoles that give rise to the higher energy RAS response of the adsorbed molecules.

The observation that the RAS of the monolayer is essentially zero across the spectral range when measured along the optical axes of the Au(110) substrate establishes that the optical dipole transitions that give rise to the spectra must be roughly orientated in a plane normal to the surface and directed along either the $[1\bar{1}0]$ or the [001] axes of the Au(110) surface [19]. This behavior has also been observed for a number of small molecules adsorbed on the Au(110) surface [19–22]. The fact that the symmetry of the substrate has such a strong influence on the structure of the monolayer and bilayer is consistent with the suggestion from the adsorption kinetics that a slower ordering process follows the initial saturation coverage.

A comparison of Figs. 2(a) and 2(b) shows that the adsorbed monolayer induces much smaller changes in the RAS of the Au(110) surface than does the adsorption of small molecules [19–22]. This is probably due to the much higher concentration of ordered dipoles on the surface produced by monolayer coverages of small molecules. From the results for saturation coverages of cytosine [19,21] and adenine [20,22] on Au(110), the dimensions of the P499C CPR molecule indicate that the number of pairs of isoalloxazine rings on a given area of the Au(110) surface will be ∼50 times lower than the number of cytosine or adenine molecules. The contribution of the isoalloxazine rings to the RAS signal will be further reduced by any spread in the alignment of the rings. However, it is notable that the weakest region of the absorption spectrum of the free molecule, 1.5–2.5 eV (Fig. 5), produces one of the strongest changes in the RAS of the Au(110) surface [Fig. 2(c)], whereas, the strongest regions of the absorption spectrum of the free molecules produce very little change in the RAS of the Au(110) surface. For example, the ratio of the peak intensities in the spectrum of the free molecules in the regions of 1.5–.5 eV, 2.5–3.5 eV, and 3.5–5.0 eV are roughly 1:5:30–75 (Fig. 5), whereas, the corresponding ratios in the RAS difference spectra of Fig. 2(c) are roughly 1:3:5. The explanation of this difference probably lies in the orientation and order of the dipoles that give rise to features in the optical spectrum of the molecules on the Au(110) surface. In the spectral region probed in these experiments, there will be two main contributions to the molecular spectrum, the isoalloxazine rings and the aromatic amino acids phenylalanine, tyrosine, and tryptophan. The spectrum of the isoalloxazine ring has been analyzed in detail [31–35] and has three main contributions, a peak at 2.7 eV, which is ∼1.0 eV wide, a band between 3.3 and 3.8 eV, and a stronger band, peaking at ∼4.6 eV. These features can be seen in the spectrum of the free molecules (Fig. 5). The dipole transitions that give rise to these features are roughly orientated along the long axis of the ring, being offset by 32°, 7°, and 29°, respectively, in one analysis [34] and 0°, 11°, and 3°, respectively, in an alternative analysis [36]. Cytochrome P450 reductase has two isoalloxazine rings, and in the "closed" fully oxidized configuration of the molecule shown in Fig. 1, the long axes of the two rings are roughly parallel to each other. If the long axes of these rings are orientated roughly vertically to the Au(110) surface as suggested in Fig. 1, then this would explain the weak contribution made to the RAS of the Au(110) surface by the features in the molecular absorption spectrum of the rings lying between 2.5 and 5.0 eV. Furthermore, the fact that the RAS of the adsorbed molecules is roughly flat when measured at an azimuthal angle (Fig. 7) of ∼90°, i.e., parallel to one of the principal axes of the Au(110), is consistent with the plane of the rings being roughly vertical to the surface. The RAS monitoring of the adsorption kinetics at energies above 2.6 eV shown in Fig. 6 could then be explained by the initial adsorption process, resulting in a configuration in which the long axes of the rings were roughly vertical to the surface and that the subsequent ordering process, revealed by the adsorption kinetics at lower RAS energies, involved only lateral movements of the molecules on the surface, perhaps facilitated by a hopping motion of the Au atoms that anchor the molecules to the surface by the Au-S bonds. Finally, while a vertical orientation of the isoalloxazine rings explains some features of the RA spectra, the angular variation results of Fig. 7 indicate that the short axes of the rings would need to be orientated roughly along one of the principal directions of the Au(110) surface $[1\bar{1}0]$ or [001] [18].

We now consider the contributions that the aromatic amino acids make to the RAS profile of the adsorbed molecules. Cytochrome P450 reductase contains 28 phenylalanine, 31 tyrosine, and 9 tryptophan amino acids, and these are widely distributed through the molecular structure of the protein [3]. These amino acid residues are expected to make a strong contribution to the two strong peaks at higher energies in the absorption spectrum of the molecule (Fig. 5). The higher energy peak may also have contributions from the peptide bonds of all the amino acids. The remarkable result is that these features are so weak in the RAS of the adsorbed molecules (Fig. 2). It is unreasonable to suppose that the weakness of these contributions to the RAS arises from all these dipoles being orientated roughly vertical to the Au(110) surface. A much more likely explanation for the weakness of these contributions is that there is no significant order in the orientation of these dipoles in the molecular structure so that, even if the molecules adopt an ordered arrangement on the Au(110) surface, there is no significant net anisotropy in the dipole orientations, resulting in a very weak RAS signal.

We noted earlier that the spectral region below 2.5 eV is very weak in the absorption spectrum of the molecule (Fig. 5) but makes one of the strongest contributions to the RAS of the adsorbed molecules (Fig. 2). We are not sure of the origin of this weak contribution to the absorption spectrum of the molecules. However, we suggest that it arises from dipole transitions in individual molecules, which become orientated in roughly the same direction during the slow ordering process that follows the initial adsorption. This would result in a net anisotropy of the optical response of the adsorbed molecules and would

explain why the intensity of this weak region of the molecular spectrum is enhanced in the RAS. It would also explain the adsorption kinetics observed at lower energies (Fig. 6).

V. CONCLUSIONS

We have determined the *p*H and concentration of the solutions required to form a monolayer and a bilayer of the mutated form P499C of human cytochrome P450 reductase on a Au(110)/electrolyte interface. The molecules are adsorbed on the Au(110) surface through a Au-S linkage. The monolayer is ordered, and the optical axes of the dipoles that contribute to an RAS signal are aligned roughly along the optical axes of the Au(110) substrate. A comparison of the RAS profile of the adsorbed monolayer with the optical absorption spectrum of the molecule in a solution shows some surprising differences. The relative intensities of the spectral regions 1.5–2.5 eV, 2.5–3.5 eV, and 3.5–5.0 eV of the molecules in a solution are roughly in the ratios 1:5:30–75, whereas, the RAS results for the same regions are roughly in the ratio 1:3:5. This indicates that there is a significant ordering on the Au(110) surface of the dipoles that give rise to the low energy region of the spectrum. The spectral contribution in the middle range arises mainly from the isoalloxazine rings, and it is suggested that this contribution to the optical response is reduced relative to the low energy region in the RAS by a roughly vertical orientation with respect to the Au(110) surface of the long axes of the rings. The high energy region of the spectrum arises from the contributions of the 68 aromatic amino acids in the molecules. This is expected to make only a weak contribution to the RAS due to the lack of any preferred orientation in the structure of the molecules of the dipoles associated with the amino acids.

Establishing the conditions necessary for the formation of an ordered monolayer of cytochrome P450 reductase on the Au(110)/electrolyte interface now makes it possible to study the dynamic behavior of this protein using RAS [8]. This will be the focus of future studies.

ACKNOWLEDGMENTS

The authors acknowledge financial support from the UK Biotechnology and Biological Science Research Council (BBSRC). J.H.C. is supported by a Ph.D. award funded by the UK Engineering and Physical Science Research Council (EPSRC). N.S.S. was supported by a Royal Society Wolfson Merit Award. The authors would also like to thank Dr. Nick Hardy from Biolin Scientific for valuable discussions in the interpretation of the QCM-D results.

[1] M. B. Murataliev, R. Feyereisen, and F. A. Walker, Biochim. Biophys. Acta **1698**, 1 (2004).
[2] A. Gutierrez, L. Y. Lian, C. R. Wolf, N. S. Scrutton, and G. C. Roberts, Biochemistry **40**, 1964 (2001).
[3] M. Wang, D. L. Roberts, R. Paschke, T. M. Shea, B. S. Siler-Masters, and J. J. P. Kim, Proc. Natl. Acad. Sci. USA **94**, 8411 (1997).
[4] A. Gutierrez, M. Paine, C. R. Wolf, N. S. Scrutton, and G. C. Roberts, Biochemistry **41**, 4626 (2002).
[5] S. Hay, S. Brenner, B. Khara, A. M. Quinn, S. E. Rigby, and N. S. Scrutton, J. Am. Chem. Soc. **132**, 9738 (2010).
[6] J. Ellis, A. Gutierrez, I. L. Barsukov, W. C. Huang, J. G. Grossmann, and G. C. Roberts, J. Biol. Chem. **284**, 36628 (2010).
[7] C. R. Pudney, B. Khara, J. O. Johannissen, and N. S. Scrutton, PLoS Biol. **9**, e1001222 (2011).
[8] H. L. Messiha, C. I. Smith, N. S. Scrutton, and P. Weightman, Europhys. Lett. **83**, 18004 (2008).
[9] D. E. Aspnes, J. P. Harbison, A. A. Studna, and L. T. Florez, J. Vac. Sci. Technol. A **6**, 1327 (1988).
[10] P. Harrison, T. Farrell, A. Maunder, C. I. Smith, and P. Weightman, Meas. Sci. Technol. **12**, 2185 (2001).
[11] Q-Sense Technology Note QS407-01-2, [www.q-sense.com].
[12] M. C. Dixon, J. Biomol. Tech. **19**, 151 (2008).
[13] I. Kamiya, D. E. Aspnes, H. Tanaka, L. T. Florez, J. P. Harbison, and R. Bhat, Phys. Rev. Lett. **68**, 627 (1992).
[14] T. Yasuda, L. Mantese, U. Rossow, and D. E. Aspnes, Phys. Rev. Lett. **74**, 3431 (1995).
[15] P. Weightman, D. S. Martin, R. J. Cole, and T. Farrell, Rep. Prog. Phys. **68**, 1251 (2005).
[16] B. Sheriden, D. S. Martin, J. R. Power, S. D. Barrett, C. I. Smith, C. A. Lucas, R. J. Nichols, and P. Weightman, Phys. Rev. Lett. **85**, 4618 (2000).
[17] B. G. Frederick, J. R. Power, R. J. Cole, C. C. Perry, Q. Chen, S. Haq, T. Bertrams, N. V. Richardson, and P. Weightman, Phys. Rev. Lett. **80**, 4490 (1998).
[18] B. G. Frederick, R. J. Cole, J. R. Power, C. C. Perry, Q. Chen, N. V. Richardson, P. Weightman, C. Verdozzi, D. R. Jennison, P. A. Schultz, and M. P. Sears, Phys. Rev. B **58**, 10883 (1998).
[19] P. Weightman, G. J. Dolan, C. I. Smith, M. C. Cuquerella, N. J. Almond, T. Farrell, D. G. Fernig, C. Edwards, and D. S. Martin, Phys. Rev. Lett. **96**, 86102 (2006).
[20] C. I. Smith, A. Bowfield, G. J. Dolan, M. C. Cuquerella, C. P. Mansley, D. G. Fernig, C. Edwards, and P. Weightman, J. Chem. Phys. **130**, 44702 (2009).
[21] C. P. Mansley, C. I. Smith, A. Bowfield, D. G. Fernig, C. Edwards, and P. Weightman, J. Chem. Phys. **132**, 214708 (2010).
[22] A. Bowfield, C. I. Smith, G. J. Dolan, M. C. Cuquerella, C. P. Mansley, and P. Weightman, e-J. Surf. Sci. Nanotechnol. **7**, 225 (2009).
[23] V. Mazine, Y. Borensztein, L. Cagon, and P. Allongue, Phys. Status Solidi A **175**, 311 (1999).
[24] V. Mazine and Y. Borensztein, Phys. Rev. Lett. **88**, 147403 (2002).
[25] P. Weightman, C. I. Smith, D. S. Martin, C. A. Lucas, R. J. Nichols, and S. D. Barrett, Phys. Rev. Lett. **92**, 199707 (2004).
[26] C. I. Smith, A. Bowfield, N. J. Almond, C. P. Mansley, J. H. Convery, and P. Weightman, J. Phys.: Condens. Matter **22**, 392001 (2010).
[27] S. Brenner, S. Hay, A. W. Munro, and N. S. Scrutton, FEBS J. **275**, 4540 (2008).
[28] Image analysis carried out using IMAGE SXM, S. D. Barrett, [http://www.ImageSXM.org.uk] (2011).

[29] R. LeParc, C. I. Smith, M. C. Cuquerella, R. L. Williams, D. G. Fernig, C. Edwards, D. S. Martin, and P. Weightman, Langmuir **22**, 3413 (2006).
[30] A. Bowfield, C. I. Smith, M. C. Cuquerella, T. Farrell, D. G. Fernig, C. Edwards, and P. Weightman, Phys. Status Solidi C **5**, 2600 (2008).
[31] B. M. della Rocca, C. I. Smith, C. Tesauro, A. Desideri, and P. Weightman, Surf. Sci. **604**, 2170 (2010).
[32] M. Sun, T. A. Moore, and P.-S. Song, J. Am. Chem. Soc. **94**, 1730 (1972).
[33] W. A. Eaton, J. Hofrichter, M. W. Makinen, R. D. Andersen, and M. L. Ludwig, Biochemistry **14**, 2146 (1975).
[34] L. B. -Å. Johansson, Å. Davidsson, G. Lindblom, and K. R. Naqvi, Biochemistry **18**, 4249 (1979).
[35] T. Climent, R. González-Luque, M. Merchán, and L. Serrano-Andrés, J. Phys. Chem. A **110**, 13584 (2006).
[36] M. Salim, U. Siddiqui, G. Kodali, and R. J. Stanley, J. Phys. Chem. B **112**, 119 (2008).
[37] C. I. Smith, A. J. Maunder, C. A. Lucas, R. J. Nichols, and P. Weightman, J. Electrochem. Soc. **150**, E233 (2003).